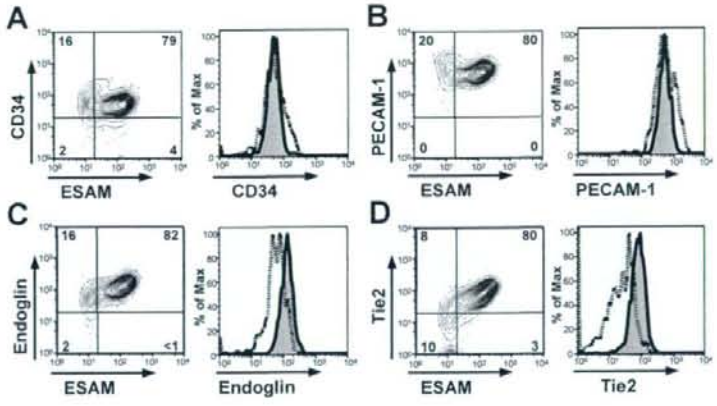
A
16
79
2
4
CD34
ESAM
% of Max
CD34
B
20
80
0
0
PECAM-1
ESAM
% of Max
PECAM-1
C
16
82
2
<1
Endoglin
ESAM
% of Max
Endoglin
D
8
80
10
3
Tie2
ESAM
% of Max
Tie2

Figure 3

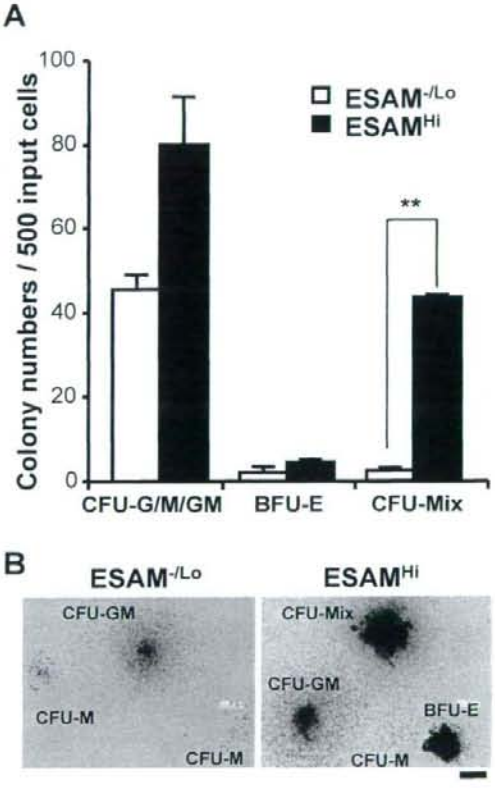
A
Colony numbers / 500 input cells
100
80
60
40
20
0
ESAM-/Lo
ESAMHi
**
CFU-G/M/GM
BFU-E
CFU-Mix
B
ESAM-/Lo
ESAMHi
CFU-GM
CFU-M
CFU-M
CFU-Mix
CFU-GM
BFU-E
CFU-M

Figure 4

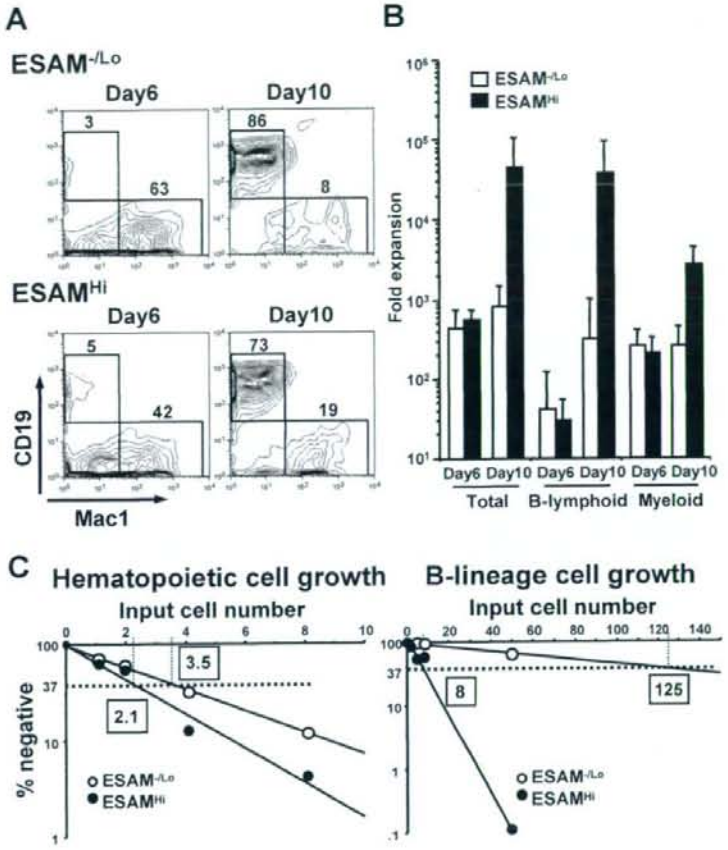
A
ESAM-/Lo
Day6
Day10
3
63
86
8
ESAMHi
Day6
Day10
5
42
73
19
CD19
Mac1
B
ESAM-/Lo
ESAMHi
Fold expansion
Day6 Day10 Day6 Day10 Day6 Day10
Total
B-lymphoid
Myeloid
C
Hematopoietic cell growth
Input cell number
% negative
3.5
2.1
ESAM-/Lo
ESAMHi
B-lineage cell growth
Input cell number
8
125
ESAM-/Lo
ESAMHi

Figure 5

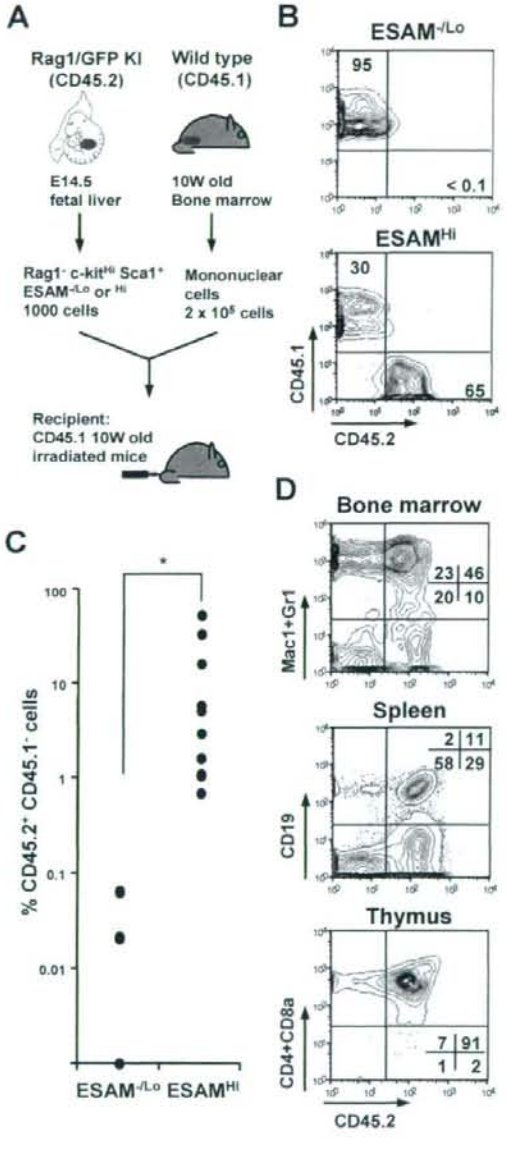
A
Rag1/GFP KI
(CD45.2)
Wild type
(CD45.1)
E14.5
fetal liver
10W old
Bone marrow
Rag1- c-kitHi Sca1+
ESAM-/Lo or Hi
1000 cells
Mononuclear
cells
2 x 10^5 cells
Recipient:
CD45.1 10W old
irradiated mice
B
ESAM-/Lo
95
< 0.1
ESAMHi
30
65
CD45.1
CD45.2
C
*
100
10
1
0.1
0.01
% CD45.2+ CD45.1- cells
ESAM-/Lo ESAMHi
D
Bone marrow
23 46
20 10
Mac1+Gr1
Spleen
2 11
58 29
CD19
Thymus
7 91
1 2
CD4+CD8a
CD45.2

Figure 6

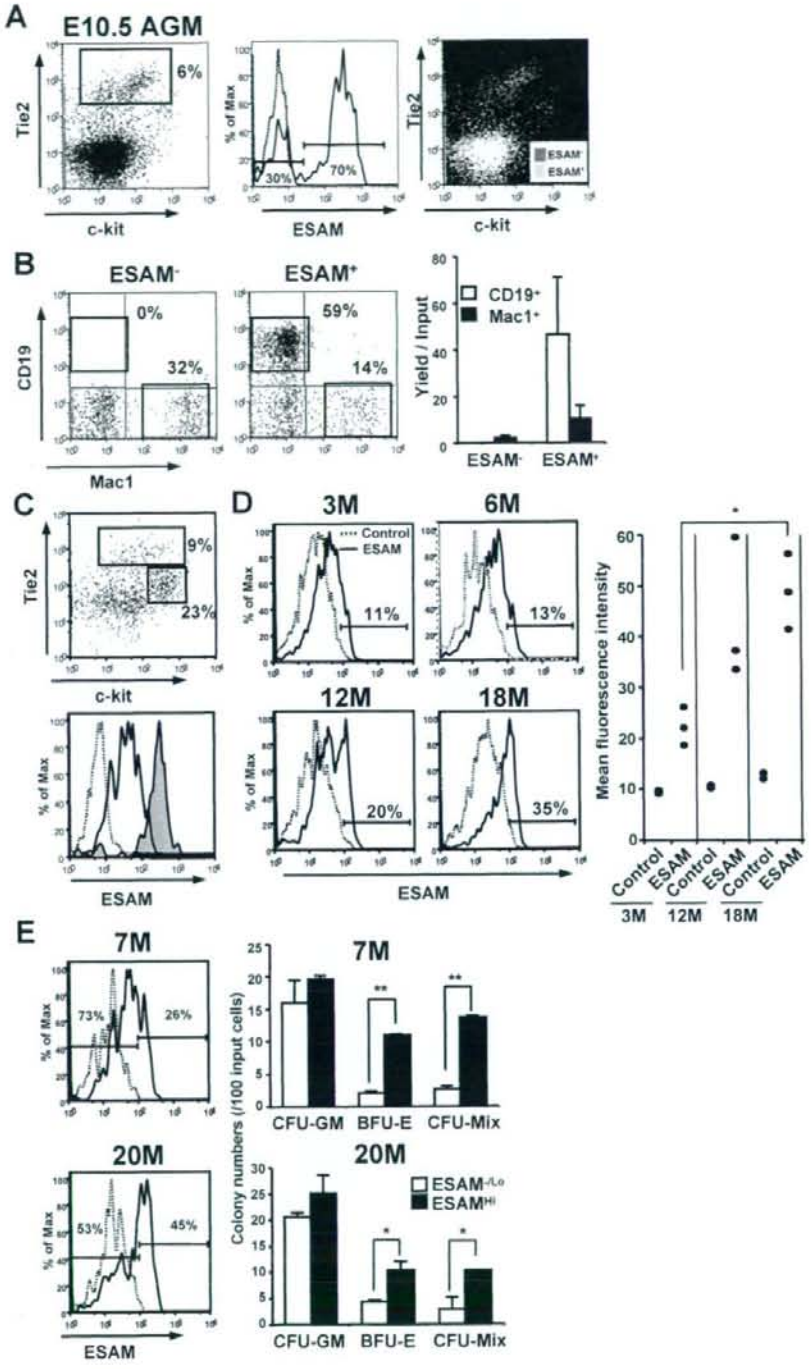
A
E10.5 AGM
Tie2
c-kit
6%
% of Max
30%
70%
ESAM
ESAM-
ESAM+
B
ESAM-
ESAM+
CD19
Mac1
0%
32%
59%
14%
CD19+
Mac1+
Yield / Input
C
9%
23%
D
3M
6M
12M
18M
Control
ESAM
11%
13%
20%
35%
Mean fluorescence intensity
E
7M
73%
26%
20M
53%
45%
CFU-GM
BFU-E
CFU-Mix
Colony numbers (/100 input cells)
ESAM-/Lo
ESAMHi

Figure 7

Ann Nucl Med (2008) 22:795–802
DOI 10.1007/s12149-008-0186-4

ORIGINAL ARTICLE

^{18}F-FDG-PET in patients with malignant lymphoma having long-term follow-up: staging and restaging, and evaluation of treatment response and recurrence

Kayako Isohashi · Mitsuaki Tatsumi · Ichiro Higuchi
Atsuo Inoue · Kazuya Nakajo · Jun Ishikawa
Eku Shimosegawa · Yuzuru Kanakura
Hironobu Nakamura · Jun Hatazawa

Received: 9 April 2008 / Accepted: 13 June 2008

Abstract
Objective The aim of this study was to evaluate the diagnostic accuracy of positron emission tomography (PET) with 2-[^{18}F]fluoro-2-deoxy-D-glucose (^{18}F-FDG) for staging/restaging, evaluating the treatment response, and screening of recurrence in patients with malignant lymphoma (ML) during long-term follow-up, and to compare that with computer tomography (CT)/magnetic resonance imaging (MRI).
Methods The study was conducted in 59 ML patients who underwent whole-body ^{18}F-FDG-PET examinations three times or more from October 1998 to August 2006. The location of the lesions in the patients with positive findings on ^{18}F-FDG-PET and/or the corresponding CT/MRI was classified into supradiaphragmatic ($n = 10$), infradiaphragmatic ($n = 7$), and extranodal sites ($n = 20$), and the findings were compared on a site basis according to the gold standard, which consisted of all clinical information available, including follow-up results.
Results A total of 156 ^{18}F-FDG-PET examinations for which the corresponding CT/MRI images were also available were evaluated, and a total of 305 sites showed positive findings on ^{18}F-FDG-PET and/or CT/MRI. Concordant positive findings were obtained in 76% for staging/restaging, 34% for evaluation of the treatment response, and 50% for screening of recurrence. The accuracy of ^{18}F-FDG-PET versus CT/MRI was 92% versus 84% ($P = 0.06$) for staging/restaging, 84% versus 50% ($P < 0.05$) for the evaluation of the treatment response, and 83% versus 72% ($P = 0.21$) for the screening of recurrence. At pathologic sites with discrepant findings between ^{18}F-FDG-PET and CT/MRI ($n = 122$), the frequency of accurate diagnosis by ^{18}F-FDG-PET (76%) was higher than that by CT/MRI (24%), especially for the evaluation of the treatment response.
Conclusions ^{18}F-FDG-PET is expected to play a significant role in the management of ML patients even after effective treatment is initiated.

Keywords Fluorodeoxyglucose · FDG · PET · Malignant lymphoma · Treatment response

K. Isohashi · I. Higuchi · A. Inoue · K. Nakajo · E. Shimosegawa · J. Hatazawa (✉)
Department of Nuclear Medicine and Tracer Kinetics, Osaka University Graduate School of Medicine, 2-2 Yamadaoka, Suita, Osaka 565-0871, Japan
e-mail: hatazawa@tracer.med.osaka-u.ac.jp

M. Tatsumi · H. Nakamura
Department of Radiology, Osaka University Graduate School of Medicine, Osaka, Japan

J. Ishikawa · Y. Kanakura
Department of Hematology and Oncology, Osaka University Graduate School of Medicine, Osaka, Japan

Introduction

Hodgkin's lymphoma (HL) accounts for less than 1% of all cases of cancer, whereas non-Hodgkin's lymphoma (NHL) accounts for about 5% of all cases of cancer [1]. Malignant lymphoma (ML) shows the characteristics of a systemic disease, and its treatment is generally dependent on chemotherapy or radiotherapy, and not on surgery. In recent years, some types of lymphoma may be curable because chemotherapy, immunotherapy, and radiotherapy have all shown remarkable advances [2, 3]. However, ML is usually characterized by repeated remissions and recurrences during the follow-up period after therapy, and patients with recurrences require

repeated courses of additional treatment. The prognosis of these patients may be improved by earlier recognition of the activity of the ML lesions and earlier institution of adequate therapy.

In recent years, positron emission tomography (PET) with 2-[^{18}F]fluoro-2-deoxy-D-glucose (^{18}F-FDG) has become a well-established modality for evaluating ML patients. In the most common types of ML (e.g., diffuse large B cell NHL, follicular NHL, mantle cell NHL, and HL) that show significant ^{18}F-FDG uptake, the sensitivity of ^{18}F-FDG-PET has been reported to exceed 80%, which is superior to that of computer tomography (CT) [2, 4–8]. In a meta-analysis of the staging methods used for ML patients, the pooled sensitivity of ^{18}F-FDG-PET was reported to be 90.9% [9]. However, to the best of our knowledge, few reports have been published on the long-term follow-up of ML patients with multiple imaging examinations [10–12]. Clinical information about ML patients undergoing long-term follow-up is of significance, and the imaging findings in relation to such information may be expected to be more reliable. We conducted a retrospective review of the ^{18}F-FDG-PET findings in ML patients undergoing long-term follow-up with multiple imaging examinations, and evaluated the diagnostic accuracy of ^{18}F-FDG-PET for staging/restaging, evaluation of the treatment response and screening of recurrence in comparison with that of CT/magnetic resonance imaging (MRI).

Table 1 Patient characteristics

Total no. of patients	59
Median age (years)	54 (range 18–78 years)
Sex	
Male	34
Female	25
Initial stage (Ann Arbor)	
I	11
II	17
III	7
IV	24
Total no. of recurrences/patients	62/35
Median follow-up in months	39 (range 12–246 months)
Patient status	
Alive/dead/unknown	41/9/9
Histology of Hodgkin's lymphoma	
Mixed cellularity	3
Nodular sclerosis	1
Histology of Non-Hodgkin's lymphoma	
Diffuse large B cell	28
Follicular	17
Mantle cell	2
Burkitt	1
Lymphoplasmacytic	1
Lymphoblastic	1
Anaplastic large cell	1
Peripheral T cell	2
Diffuse mixed B cell	1
True histiocytic	1

Materials and methods

Patients

This study included 59 ML patients who underwent whole-body ^{18}F-FDG-PET examinations three times or more from October 1998 to August 2006. A total of 227 ^{18}F-FDG-PET examinations were performed on these patients. The diagnosis of ML had been confirmed histopathologically in all the patients. There were 34 men and 25 women patients (median age 54 years; range 18–78); 4 patients had HL, and 55 had NHL. The patient characteristics are presented in Table 1. All patients gave an informed consent for both the ^{18}F-FDG-PET and CT/MRI examinations.

^{18}F-FDG-PET study

A whole-body PET using ^{18}F-FDG was performed with a Headtome-V/SET 2400 W PET System (Shimadzu, Kyoto, Japan). This device provided 47 slices with center-to-center distances of 3.125 mm. The intrinsic spatial resolution was 4.0 mm in plane and 4.3 mm full-width at half-maximum axially. Reconstruction with a Butterworth filter resulted in a final in-plane resolution of approximately 8 mm full-width at half-maximum. Data were acquired in the two-dimensional mode. All emission data were corrected for tissue attenuation by means of transmission scan with an external source of ^{68}Ge–^{68}Ga [13]. After at least 4 h of fasting, adult patients received an intravenous injection of approximately 370 MBq of ^{18}F-FDG.

Image interpretation

All ^{18}F-FDG-PET and CT/MRI were performed at the same nuclear medicine/radiology department and interpreted respectively by the radiologist of the same team blinded to patient outcome, referring to the results of individual imaging reports. In all ^{18}F-FDG-PET images, any obvious foci of increased ^{18}F-FDG uptake over the background (i.e., blood pool) not located in areas of normal ^{18}F-FDG uptake and/or excretion were considered positive for tumor [14, 15]. In all the CT/MRI images, lymph nodes (LNs) seen on CT/MRI were measured by their two-dimensional diameter in the transverse plane. The CT/MRI images were examined for anatomical abnormalities (e.g., swelling of individual organs, space

occupying lesion (SOL) in individual organs, soft-tissue density), as well as abnormal contrast enhancement patterns of solid organs, which were considered to be suspect lesions. For the purpose of staging and restaging, standard CT/MRI size criteria for individual LN groups were used to evaluate pathologic LNs, whereby LNs greater than 10 mm in the short axis diameter were considered to be positive [16, 17]. Treatment response on CT/MRI was assessed by the criteria proposed at the Cotswold Meeting for HL and the International Working Group for NHL [18, 19], as follows. Complete remission: regression of all the LNs to their normal size (≤1.5 cm in their greatest transverse diameter for nodes >1.5 cm before therapy), decrease in the size of nodes measuring 1.1–1.5 cm in their greatest transverse diameter before therapy to ≤1 cm after treatment, or regression by more than 75% of the sum of the products of the greatest diameters of the LNs; partial remission: regression by more than 50% of the sum of the products of the greatest diameters of the six largest dominant nodes or nodal masses. No increase in the size of the other nodes, liver, or spleen, and no new sites of disease. In the screening to detect recurrence, the criteria proposed at the Cotswold Meeting for HL, the International Working Group for NHL, and the Response Definitions for Clinical Trials were referred to [15, 18–20]. The appearance of any new lesion and/or increase in size of prior lesions was considered to represent disease relapse.

Data analysis

The objective of each ^{18}F-FDG-PET examination was classified into staging/restaging, evaluation of treatment response, or screening of recurrence. In this study, restaging was defined as evaluation of the extent of recurrence just prior to treatment. The locations of positive findings on ^{18}F-FDG-PET and/or corresponding CT/MRI which were performed within at least 1 month, without intervening treatment, were classified into the following 48 anatomic sites: 10 supradiaphragmatic regions, including the right and left cervical, right and left clavicular, right and left axillary, right and left hilar, mediastinal, retrocrural, 7 infradiaphragmatic regions, including paraaortic–iliac, mesenteric, right and left pelvic, right and left inguinal, and other abdominal sites, 20 extranodal regions, including maxilla-orbit, tonsil, thyroid, cervical spine, right and left lung, breast, chest wall, liver, spleen, right and left adrenal, stomach, duodenum, colon, rectum, uterus, abdominal wall, bone, and subcutaneous sites. For each of the examination objectives, these findings were compared on a site basis according to the gold standard, which consisted of all clinical information available, including the results of the follow-up. For each of the examination objectives, the rate of concordant positive findings was estimated and the accuracy of ^{18}F-FDG-PET versus CT/MRI was evaluated. The sites showing discrepant findings were also analyzed, and the frequency of correct diagnosis by ^{18}F-FDG-PET in relation to the discrepant findings was evaluated. The advantages or disadvantages of ^{18}F-FDG-PET conducted during follow-up on the patient management were also evaluated in comparison with the corresponding CT/MRI and the clinical information obtained from individual medical records.

Of the 227 ^{18}F-FDG-PET examinations, 156 had corresponding CT/MRI performed; 53 of the 156 ^{18}F-FDG-PET examinations were performed to evaluate staging/restaging, 71 to evaluate the treatment response, and 32 for screening of recurrence. The 53 ^{18}F-FDG-PET examinations for staging/restaging were compared with the corresponding CT (neck 28, chest 45, and abdomen 44) examinations and 6 MRI (brain 1, spine 3, upper abdomen 1, and pelvic 1) examinations. The 71 ^{18}F-FDG-PET examinations obtained for evaluation of the treatment response were compared with the corresponding CT (neck 11, chest 28, and abdomen 44) examinations and 6 MRI (spine 2 and pelvic 4) examinations. The 32 ^{18}F-FDG-PET examinations obtained for screening of recurrence were compared with the corresponding CT (neck 9, chest 14, and abdomen 18) examinations and 6 MRI (spine 3 and pelvic 3) examinations.

Statistical analysis

McNemar's test was used to analyze the symmetry, and P values were evaluated in relation to the accuracy; P values of less than 0.05 were considered to be statistically significant.

Results

A total of 305 sites, 171 in the examinations for staging/restaging, 88 in the examinations for evaluation of treatment response, and 46 in the examinations for screening of recurrence, showed positive findings on ^{18}F-FDG-PET and/or CT/MRI. Concordant positive findings were obtained in 76% (130/171 anatomic sites) for staging/restaging, 34% (30/88) for evaluation of treatment response and 50% (23/46) for screening of recurrence. Two sites showed false-positive findings on both ^{18}F-FDG-PET and CT. In one, the lesion was located in the ileocolic wall, and was diagnosed as true negative on MRI. In the other, the lesion was located in the liver, and in this case, false-positive findings were also obtained on MRI.

Table 2 Concordant positive findings and the accuracy of 2-[^{18}F]fluoro-2-deoxy-D-glucose positron emission tomography (^{18}F-FDG-PET) and computer tomography (CT)/magnetic resonance imaging (MRI)

Purpose	Concordant positive findings (%) (number[a])	Accuracy of ^{18}F-FDG PET (%)	Accuracy of CT/MRI (%)	*P*
Staging/restaging	76 (130/171)	92	84	0.06
Evaluation of treatment response	34 (30/88)	84	50	<0.01
Screening of recurrence	50 (23/46)	83	72	0.21

[a]Number of concordant sites/total sites

Table 3 Evaluation of discrepant findings between ^{18}F-FDG-PET and CT/MRI

Purpose	Number of discrepant sites	Frequency of correct diagnosis by ^{18}F-FDG-PET (%)
Staging/restaging	41	66
Evaluation of treatment response	58	76
Screening of recurrence	23	65

The accuracy of ^{18}F-FDG-PET versus CT/MRI was 92% versus 84% for staging/restaging, 84% versus 50% for evaluation of treatment response, and 83% versus 72% for screening of recurrence, respectively. The accuracy of ^{18}F-FDG-PET was significantly superior to that of CT/MRI for evaluation of the treatment response ($P < 0.01$). Table 2 shows a summary of the results.

The sites showing discrepant findings between ^{18}F-FDG-PET and CT/MRI were analyzed. The frequency of correct diagnosis by ^{18}F-FDG-PET was 27 of 41 for staging/restaging, 44 of 58 for evaluation of treatment response, and 15 of 23 for screening of recurrence (66%, 76%, and 65%, respectively). The details are shown in Table 3.

The lesions at these sites showing discrepant findings were further analyzed. For staging/restaging, normal-sized LN lesions (18 sites) were correctly diagnosed as true positive by ^{18}F-FDG-PET, whereas pulmonary involvement (six sites) was correctly diagnosed as true positive by CT (Fig. 1). Normal-sized LN lesions located in the neck, supraclavicular, and inguinal regions on CT/MRI tended to be diagnosed as true positive by ^{18}F-FDG-PET, whereas large-sized LN lesions located in the axillary region on CT/MRI tended to be diagnosed as true negative by ^{18}F-FDG-PET. For evaluation of the treatment response, post-treatment scars (31 sites), such as abnormal soft tissue or residual mass seen on CT/MRI were correctly diagnosed as true negative using ^{18}F-FDG-PET (Fig. 2), whereas pulmonary involvement (four sites) was correctly diagnosed as true positive using CT. Residual post-treatment scars in the paraaortic–iliac, mediastinal, and mesenteric regions and in the stomach on CT/MRI tended to be diagnosed as true negative by ^{18}F-FDG-PET. For screening of recurrence, normal-sized LN lesions (10 sites) were correctly diagnosed as true positive using ^{18}F-FDG-PET, whereas hepatic involvement (two sites) was correctly diagnosed as true positive using CT/MRI. Normal-sized LN lesions located in the neck, supraclavicular, and paraaortic regions on CT/MRI tended to be diagnosed as true positive by ^{18}F-FDG-PET.

Examination-based analysis revealed that the advantages of ^{18}F-FDG-PET performed during the course of follow-up of ML included correct staging (down: 1 examination) and restaging (up: 2 examinations), earlier recognition of complete remission (24 examinations) and partial remission (1 examination), correct evaluation of residual tumor under treatment (2 examinations), detection of recurrence under treatment (1 examination), and earlier detection of recurrence (4 examinations; Fig. 3), and disease extension (1 examination). The ^{18}F-FDG-PET exhibited incorrect evaluation as understaging (3 examinations), overstaging (1 examination), false-negative finding of complete remission (1 examination), and false-positive findings after treatment (6 examinations).

Discussion

This study demonstrated that the treatment response in patients with ML can be evaluated more accurately by ^{18}F-FDG-PET than by CT/MRI.

The course of ML, even after radio-, chemo- and/or chemoradiotherapy, is characterized by repeated remissions and recurrences throughout the follow-up period. In recent years, ^{18}F-FDG-PET and CT/MRI have frequently been used as the first-line imaging modality for evaluating ML patients. The accuracy of ^{18}F-FDG-PET for disease staging was reported to be 94% in patients with HL and NHL, and that of CT 60% in patients with HL and 73% in patients with NHL [5]. In relation to therapy monitoring, the accuracy of ^{18}F-FDG-PET versus CT was reported to be 85% versus 54% [21]. For restaging, which was equal to the follow-up evaluation

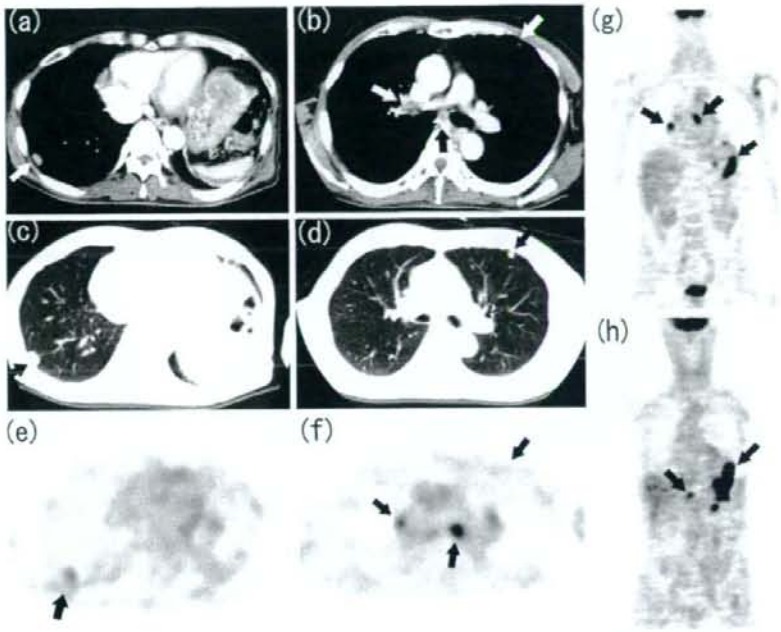

Fig. 1 2-[^{18}F]fluoro-2-deoxy-D-glucose positron emission tomography (^{18}F-FDG-PET) and computer tomography (CT) images obtained for restaging in a 63-year-old man with recurrence of diffuse large B cell lymphoma (DLBCL). Axial CT images showing nodules in the right lung S9 (15 mm, **a**, **c**) and the left lung S3 (6 mm, **b**, **d**). Axial ^{18}F-FDG-PET images showing abnormal ^{18}F-FDG uptake in the nodule of the right lung S9 (**e**), but no abnormal uptake in the nodule of the left lung S3 (**f**). Coronal ^{18}F-FDG-PET images showing abnormal ^{18}F-FDG uptake in the mediastinal, right hilar and porta hepatis regions, and stomach (**g**, **h**). *Arrows* on CT and/or ^{18}F-FDG-PET show involvement of DLBCL

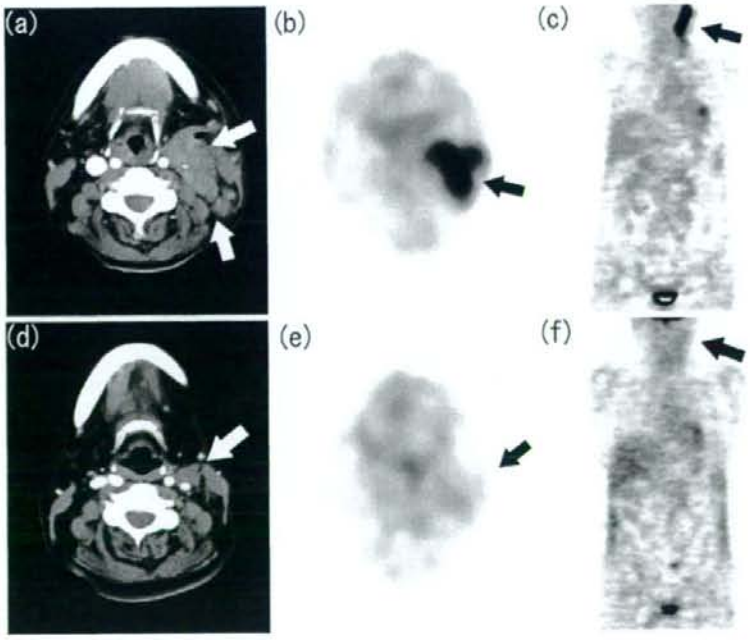

Fig. 2 ^{18}F-FDG-PET and CT images obtained for restaging (**a**–**c**) and evaluation of treatment response (**d**–**f**) in a 51-year-old woman with recurrence of lymphoplasmacytic lymphoma. Axial and coronal ^{18}F-FDG-PET images (**b**, **c**) obtained for restaging showing abnormal ^{18}F-FDG uptake in the left neck (*black arrows*), and the axial CT image (**a**) showing massive involvement in the left neck (*white arrows*). After chemotherapy, the axial and coronal ^{18}F-FDG-PET images (**e**, **f**) were negative (*black arrows*), but the axial CT image (**d**) showed residual soft-tissue density (*white arrow*). This patient was considered to be in complete remission on the basis of the clinical follow-up results

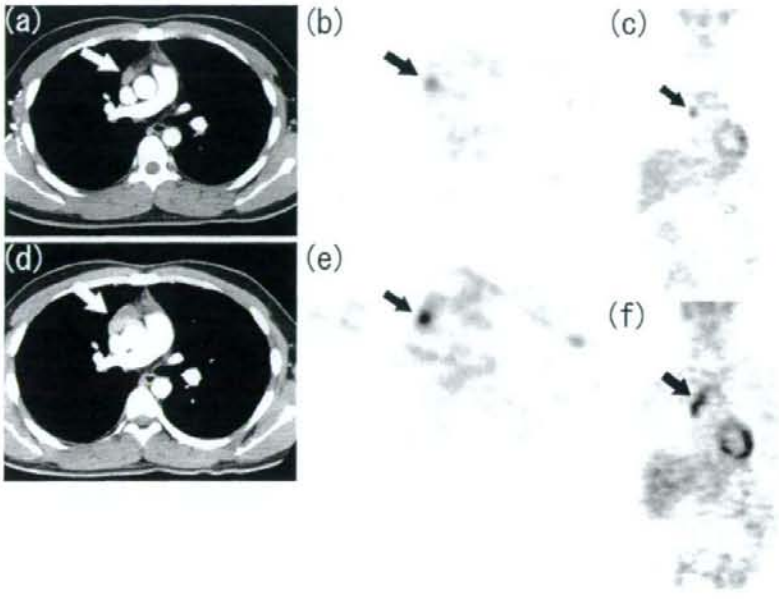

Fig. 3 CT and ^{18}F-FDG-PET images obtained for screening of recurrence (**a**–**c**) and those obtained 18 months later (**d**–**f**) in an 18-year-old man with recurrence of HL (nodular sclerosis type). Axial and coronal ^{18}F-FDG-PET images (**b**, **c**) for screening of recurrence showing abnormal ^{18}F-FDG uptake in the mediastinal region (*black arrows*). The axial CT image (**a**) showing residual soft-tissue density (*white arrow*), which remained unchanged as compared with that in the previous CT images. The patient was asymptomatic, and was followed up carefully. Eighteen months later, axial and coronal ^{18}F-FDG-PET images (**e**, **f**) showed more intense uptake (*black arrows*). The axial CT image (**d**) also showed enlargement of the soft-tissue mass, with abnormal contrast enhancement inside the mass (*white arrow*)

in this study, the accuracy of ^{18}F-FDG-PET versus CT was reported to be 95% versus 84% [10]. Our results for the patients with ML having long-term follow-up and receiving multiple imaging examinations were consistent with those of these prior reports.

The concordance in staging between ^{18}F-FDG-PET and CT was reported to be 80–90% [4, 22]. In relation to staging/restaging, 83% of the discrepant findings between ^{18}F-FDG-PET and CT were accurately diagnosed by ^{18}F-FDG-PET [2]. This study demonstrated that the frequency of concordant positive findings between ^{18}F-FDG-PET and CT/MRI was especially low in relation to the treatment response, and most of the discrepant findings were correctly diagnosed by ^{18}F-FDG-PET. It has been reported that alterations in glucose metabolism become evident earlier than morphologic alterations [23–26]. Therefore, ^{18}F-FDG-PET is useful to predict the effectiveness of treatment and complete remission earlier than that allowed by CT/MRI in cases of ML [15, 20, 27].

In this study, some cases showed residual masses or abnormal soft tissue densities/intensities after treatment induction for lymphoma, and it was difficult to distinguish between viable tumor and necrosis or fibrosis in these lesions on CT/MRI. However, most of these cases were diagnosed correctly as complete remission (CR) by ^{18}F-FDG-PET. A number of prior studies have reported the ability of ^{18}F-FDG-PET to distinguish between viable lymphoma and necrosis or fibrosis in residual masses following treatment of HL and aggressive NHL [5, 10, 12, 20, 25, 28–31]. Our results for the patients with ML having long-term follow-up and receiving multiple imaging examinations were consistent with those of these prior reports.

In recent years, follow-up ^{18}F-FDG-PET studies have been recommended for patients with ML [14, 19, 32, 33]. However, the usefulness of ^{18}F-FDG-PET in the follow-up of ML patients is yet to be determined. Although the number of patients was small, we were able to recognize ML recurrence earlier in four cases using ^{18}F-FDG-PET.

Our results indicated that the frequency of accurate diagnosis by ^{18}F-FDG-PET was superior to that by CT/MRI for all purposes, especially for the evaluation of

treatment response. However, ^{18}F-FDG-PET had some limitations, and there were cases in which CT/MRI proved to be better. ^{18}F-FDG-PET tended to miss small tumor foci because of its limited spatial resolution. Small pulmonary involvement was often missed on ^{18}F-FDG-PET images in our study. Hepatic involvement not detectable on ^{18}F-FDG-PET images was accurately diagnosed by CT/MRI in two patients. In addition, for patients with subtypes showing a variably ^{18}F-FDG avid and FDG-avidity unknown such as mucosa-associated lymphoid tissue, lesions should be evaluated with CT/MRI if a pretreatment ^{18}F-FDG-PET was not performed or was negative [15, 34, 35].

The ^{18}F-FDG-PET/CT, a combined metabolic and morphologic imaging modality, has been widely used in clinical practice in recent years. With coregistration of ^{18}F-FDG-PET and CT, an anatomical position of abnormal accumulation is identified easily, and even in the case with equivocal or no accumulation, abnormal lesions are detected with the help of CT. Although the CT portion of ^{18}F-FDG-PET/CT is usually low-dose non-enhanced CT, it is reported that the sensitivity and the specificity of ^{18}F-FDG-PET/CT are better than those of contrast-enhanced CT in evaluating LN and organ involvement in HL or aggressive NHL [1, 36].

There were several limitations of this study. First, not all the presumed lesions were confirmed histopathologically. Most of the lesions were compared on a site basis according to the gold standard, which consisted of all the clinical information available, including the results of follow-up, instead of by biopsy. Second, the patient population was composed of patients with different HL and NHL subtypes, and the numbers of patients with some subtypes were limited. In this study, the majority of the ML population included patients with diffuse large B cell lymphoma (DLBCL) and the follicular subtype of lymphoma, subtypes which are known to show a significant ^{18}F-FDG uptake. Third, the number and interval or area of ^{18}F-FDG-PET and CT/MRI examinations performed actually at the same nuclear medicine/radiology department varied between ML patients. In the same patient, to compare the clinical course with more examinations, ML patients who underwent ^{18}F-FDG-PET examinations more than three times at least were selected in this study.

Conclusions

In spite of the several limitations of this study, we concluded that ^{18}F-FDG-PET exhibited higher accuracy than CT/MRI for evaluation of the treatment response of ML. Thus, ^{18}F-FDG-PET is expected to play a significant role in the management of ML patients even after effective treatment is initiated.

Acknowledgments This study was partly supported by a grant for Basic Research in Health and Welfare, National Institute of Biomedical Innovation (J060701435 and J070701433).

References

1. von Schulthess GK, Steinert HC, Hany TF. Integrated PET/CT: current applications and future directions. Radiology 2006;238:405–22.
2. Tatsumi M, Cohade C, Nakamoto Y, Fishman EK, Wahl RL. Direct comparison of FDG PET and CT findings in patients with lymphoma: initial experience. Radiology 2005;237:1038–45.
3. Mikhaeel NG. Use of FDG-PET to monitor response to chemotherapy and radiotherapy in patients with lymphomas. Eur J Nucl Med Mol Imaging 2006;33:22–6.
4. Moog F, Bangerter M, Diederichs CG, Guhlmann A, Merkle E, Frickhofen N, et al. Extranodal malignant lymphoma: detection with FDG PET versus CT. Radiology 1998;206:475–81.
5. Stumpe KD, Urbinelli M, Steinert HC, Glanzmann C, Buck A, von Schulthess GK. Whole-body positron emission tomography using fluorodeoxyglucose for staging of lymphoma: effectiveness and comparison with computed tomography. Eur J Nucl Med Mol Imaging 1998;25:721–8.
6. Newman JS, Francis IR, Kaminski MS, Wahl RL. Imaging of lymphoma with PET with 2-[F-18]-fluoro-2-deoxy-D-glucose: correlation with CT. Radiology 1994;190:111–6.
7. Thill R, Neureburg J, Fabry U, Cremerius U, Wagenknecht G, Hellwig D, et al. Comparison of findings with 18-FDG PET and CT in pretherapeutic staging of malignant lymphoma. Nuklearmedizin 1997;36:234–9.
8. Buchmann I, Reinhardt M, Elsner K, Bunjes D, Altehoefer C, Finke J, et al. 2-(fluorine-18)fluoro-2-deoxy-D-glucose positron emission tomography in the detection and staging of malignant lymphoma. A bicenter trial. Cancer 2001;91:889–99.
9. Isasi CR, Lu P, Blaufox MD. A metaanalysis of ^{18}F-2-deoxy-2-fluoro-D-glucose positron emission tomography in the staging and restaging of patients with lymphoma. Cancer 2005;104:1066–74.
10. Freudenberg LS, Antoch G, Schütt P, Beyer T, Jentzen W, Müller SP, et al. FDG-PET/CT in re-staging of patients with lymphoma. Eur J Nucl Med Mol Imaging 2004;31:325–9.
11. Talbot JN, Haioun C, Rain JD, Meignan M, Wioland M, Misset JL, et al. [18F]-FDG positron imaging in clinical management of lymphoma patients. Crit Rev Oncol Hematol 2001;38:193–221.
12. Spaepen K, Stroobants S, Dupont P, Van Steenweghen S, Thomas J, Vandenberghe P, et al. Prognostic value of positron emission tomography (PET) with fluorine-18 fluorodeoxyglucose ([18F]FDG) after first-line chemotherapy in non-Hodgkin's lymphoma: is [18F]FDG-PET a valid alternative to conventional diagnostic methods? J Clin Oncol 2001;19:414–9.
13. Iida H, Miura S, Shoji Y, Ogawa T, Kado H, Narita Y, et al. Noninvasive quantitation of cerebral blood flow using oxygen-15-water and a dual-PET system. J Nucl Med 1998;39:1789–98.

14. Juweid ME, Stroobants S, Hoekstra OS, Mottaghy FM, Dietlein M, Guermazi A, et al. Use of positron emission tomography for response assessment of lymphoma: consensus of the Imaging Subcommittee of International Harmonization Project in Lymphoma. J Clin Oncol 2007;25:571–8.
15. Cheson BD, Pfistner B, Juweid ME, Gascoyne RD, Specht L, Horning SJ, et al. Revised response criteria for malignant lymphoma. J Clin Oncol 2007;25:579–86.
16. Dorfman RE, Alpern MB, Gross BH, Sandler MA. Upper abdominal lymph nodes: criteria for normal size determined with CT. Radiology 1991;180:319–22.
17. Glazer GM, Gross BH, Quint LE, Francis IR, Bookstein FL, Orringer MB. Normal mediastinal lymph nodes: number and size according to American Thoracic Society mapping. Am J Roentgenol 1985;144:261–5.
18. Lister TA, Crowther D, Sutcliffe SB, Glatstein E, Canellos GP, Young RC, et al. Report of a committee convened to discuss the evaluation and staging of patients with Hodgkin's disease: Cotswolds meeting. J Clin Oncol 1989;7:1630–6.
19. Cheson BD, Horning SJ, Coiffier B, Shipp MA, Fisher RI, Connors JM, et al. Report of an international workshop to standardise response criteria for non-Hodgkin's lymphomas. NCI Sponsored International Working Group. J Clin Oncol 1999;17:1244–53.
20. Juweid ME, Wiseman GA, Vose JM, Ritchie JM, Menda Y, Wooldridge JE, et al. Response assessment of aggressive non-Hodgkin's lymphoma by integrated International Workshop Criteria and fluorine-18-fluorodeoxyglucose positron emission tomography. J Clin Oncol 2005;23:4652–61.
21. Cremerius U, Fabry U, Kröll U, Zimny M, Neuerburg J, Osieka R, et al. Clinical value of FDG PET for therapy monitoring of malignant lymphoma: results of a retrospective study in 72 patients. Nuklearmedizin 1999;38:24–30.
22. Juweid G, Beguin Y, Najjar F, Hustinx R, Fassotte MF, Rigo P, et al. Positron emission tomography (PET) with 18F-fluorodeoxyglucose (18F-FDG) for the staging of low grade non-Hodgkin's lymphoma (NHL). Ann Oncol 2001;12:825–30.
23. Wahl RL, Zasadny K, Helvie M, Hutchins GD, Weber B, Cody R. Metabolic monitoring of breast cancer chemohormonotherapy using positron emission tomography: initial evaluation. J Clin Oncol 1993;11:2101–11.
24. Canellos GP. Residual mass in lymphoma may not be residual disease. J Clin Oncol 1988;6:931–3.
25. Jerusalem G, Beguin Y, Fassotte MF, Najjar F, Paulus P, Rigo P, et al. Whole-body positron emission tomography using 18F-fluorodeoxyglucose for posttreatment evaluation in Hodgkin's disease and non-Hodgkin's lymphoma has higher diagnostic and prognostic value than classical computed tomography scan imaging. Blood 1999;94:429–33.
26. Kostakoglu L, Goldsmith SJ. Fluorine-18 fluorodeoxyglucose positron emission tomography in the staging and follow-up of lymphoma: is it time to shift gears? Eur J Nucl Med Mol Imaging 2000;27:1564–78.
27. Kumar R, Maillard I, Schuster SJ, Alavi A. Utility of fluorodeoxyglucose-PET imaging in the management of patients with Hodgkin's and non-Hodgkin's lymphomas. Radiol Clin North Am 2004;42:1083–100.
28. Lavely WC, Delbeke D, Greer JP, Morgan DS, Byrne DW, Price RR, et al. FDG PET in the follow-up management of patients with newly diagnosed Hodgkin and non-Hodgkin lymphoma after first-line chemotherapy. Int J Radiat Oncol Biol Phys 2003;57:307–15.
29. Jerusalem G, Warland V, Najjar F, Paulus P, Fassotte MF, Fillet G, et al. Whole-body 18F-FDG PET for the evaluation of patients with Hodgkin's disease and non-Hodgkin's lymphoma. Nucl Med Commun 1999;20:13–20.
30. Cremerius U, Fabry U, Neuerburg J, Zimny M, Osieka R, Buell U. Positron emission tomography with 18F-FDG to detect residual disease after therapy for malignant lymphoma. Nucl Med Commun 1998;19:1055–63.
31. Specht L. 2-[18F]fluoro-2-deoxyglucose positron-emission tomography in staging, response evaluation, and treatment planning of lymphomas. Semin Radiat Oncol 2007;17:190–7.
32. Hoppe RT, Advani RH, Bierman PJ, Bloomfield CD, Buadi F, Djulgegovic B, et al. Hodgkin disease/lymphoma. Clinical practice guidelines in oncology. J Natl Compr Canc Netw 2006;4:210–30.
33. Zelenetz AD, Advani RH, Buadi F, Cabanillas F, Caligiuri MA, Czuczman MS, et al. Non-Hodgkin's lymphoma. Clinical practice guidelines in oncology. J Natl Compr Canc Netw 2006;4:258–310.
34. Hoffmann M, Wöhrer S, Becherer A, Chott A, Streubel B, Kletter K, et al. 18F-Fluoro-deoxy-glucose positron emission tomography in lymphoma of mucosa-associated lymphoid tissue: histology makes the difference. Ann Oncol 2006;17:1761–5.
35. Enomoto K, Hamada K, Inohara H, Higuchi I, Tomita Y, Kubo T, et al. Mucosa-associated lymphoid tissue lymphoma studied with FDG-PET: a comparison with CT and endoscopic findings. Ann Nucl Med 2008;22:261–7.
36. Schaefer NG, Hany TF, Schaefer NG, Hany TF, Taverna C, Seifert B, et al. Non-Hodgkin lymphoma and Hodgkin disease: coregistered FDG PET and CT at staging and restaging—do we need contrast-enhanced CT? Radiology 2004;232:823–9.

THE JOURNAL OF BIOLOGICAL CHEMISTRY VOL. 283, NO. 44, pp. 30045–30056, October 31, 2008

AML1/RUNX1 Works as a Negative Regulator of c-Mpl in Hematopoietic Stem Cells*

Received for publication, June 23, 2008, and in revised form, August 6, 2008 Published, JBC Papers in Press, August 7, 2008, DOI 10.1074/jbc.M804768200

Yusuke Satoh[‡], Itaru Matsumura[‡1], Hirokazu Tanaka[‡], Sachiko Ezoe[‡], Kentaro Fukushima[‡], Masahiro Tokunaga[‡], Masato Yasumi[‡], Hirohiko Shibayama[‡], Masao Mizuki[‡], Takumi Era[§], Tsukasa Okuda[¶], and Yuzuru Kanakura[‡]

From the [‡]Department of Hematology and Oncology, Osaka University Graduate School of Medicine, 2-2 Yamada-oka, Suita, Osaka 565-0871, the [§]Division of Molecular Neurobiology, Institute of Molecular Embryology and Genetics, Kumamoto University, Kumamoto 860-0811, and the [¶]Department of Biochemistry and Molecular Biology, Kyoto Prefectural University of Medicine, Kyoto 602-8566, Japan

In this study, we analyzed the roles for AML1/RUNX1 in the regulation of the c-*mpl* promoter. Wild-type AML1 activated the c-*mpl* promoter through the proximal AML-binding site in luciferase assays using 293T and HeLa cells. In accord with this result, electrophoretic mobility shift assay and chromatin immunoprecipitation assays demonstrated that AML1 bound to this site. Next, we analyzed the function of AML1 using a mutant of AML1 lacking the C terminus (AML1dC), which was originally found in a patient with myelodysplastic syndromes. AML1dC dominant-negatively suppressed transcriptional activity of wild-type AML1. However, unexpectedly, AML1dC-transduced murine c-Kit$^+$Sca1$^+$Lineage$^-$ cells expressed c-*mpl* mRNA and c-Mpl protein more abundantly than mock-transduced cells, which led to the enhanced thrombopoietin-mediated proliferation. Moreover, when AML1dC was induced to express during the development of hematopoietic cells from embryonic stem (ES) cells, AML1dC augmented the c-Mpl expression on hematopoietic stem/progenitor cells. Furthermore, we found that early hematopoietic cells that derived from AML1$^{+/-}$ ES cells expressed c-Mpl more intensely than those that developed from wild-type ES cells. In contrast, AML1dC hardly affected c-Mpl expression and maturation of megakaryocytes. As for the mechanism of the different roles of AML1 in the regulation of the c-*mpl* promoter, we found that AML1 forms a complex with a transcription repressor mSin3A on the c-*mpl* promoter in hematopoietic stem/progenitor cells, although it forms a complex with a transcription activator p300 on the same promoter in megakaryocytic cells. Together, these data indicate that AML1 can regulate the c-*mpl* promoter both positively and negatively by changing the binding partner according to cell types.

AML1 (RUNX1) is a family member of heterodimeric transcription factors named core binding factors. *AML1* was originally identified at a breakpoint on human chromosome 21 in the t(8;21) translocation and known as the most common targets of chromosomal translocations in human leukemia (1, 2). In addition to chromosomal translocations, recent reports have shown the importance of point mutations of AML1 in hematological malignancies, such as acute myelogenous leukemia (AML)[2] and myelodysplastic syndromes (MDS) (3). The Runt domain of AML1 is utilized for DNA binding and heterodimerization with a partner PEBP2β/CBFβ. Although PEBP2β by itself does not bind to the DNA, the association with PEBP2β is necessary for AML1 to elicit its biologic activity (4–6). AML1 can regulate the transcription of the target gene both positively and negatively through the binding to the consensus DNA sequence, TGT/cGGT, possibly dependent on the cellular context and/or its target gene. For example, it positively regulates the expression cytokines and their receptors in myeloid and lymphoid lineage cells (7–12), whereas it negatively regulates CD4 transcription in immature thymocytes (13). Several experiments using conventional and conditional gene targeting in mice demonstrated that AML1 is essential for the early step in definitive hematopoiesis (14). North *et al.* (15) revealed that AML1 is required for the generation of hematopoietic stem cells (HSCs) from the vitelline and umbilical arteries and from the aorta-gonad-mesonephros (AGM) region. In addition, AML1 is necessary for the transitions from the stage of double-negative (DN)2 to DN3 and DN3 to DN4 in the T-lymphocyte development (9, 17). Furthermore, AML1 plays an important role in the maturation of megakaryocytes and platelet production. AML1 deletion in adult mice led to the impaired polyploidization of megakaryocytes and low platelet production (17, 18), whereas the number of megakaryocyte progenitors was not altered in these mice, suggesting that AML1 is indispensable for the terminal maturation of megakaryocytes. Also, the hereditary loss-of-function mutation of AML1 or

* This work was supported by grants from the Ministry of Education, Science, Sports, and Culture and Technology of Japan and the Sankyo Foundation of Life Science. The costs of publication of this article were defrayed in part by the payment of page charges. This article must therefore be hereby marked "*advertisement*" in accordance with 18 U.S.C. Section 1734 solely to indicate this fact.

[1] To whom correspondence should be addressed. Tel.: 81-6-6879-3871; Fax: 81-6-6879-3879; E-mail: matumura@bldon.med.osaka-u.ac.jp.

[2] The abbreviations used are: AML, acute myelogenous leukemia; HSC, hematopoietic stem cells; EMSA, electrophoretic mobility shift assay; ES, embryonic stem cell; TPO, thrombopoietin; ChIP, chromatin immunoprecipitation; FACS, fluorescence-activated cell sorter; DMEM, Dulbecco's modified Eagle's medium; FBS, fetal bovine serum; Ab, antibody; MDS, myelodysplastic syndrome; FITC, fluorescein isothiocyanate; CLP, common lymphoid progenitor; GFP, green fluorescent protein; RT, reverse transcription; DN, double-negative; h, human; m, murine; IL, interleukin; WT, wild type; MT, mutant; Tet, tetracycline; SCF, stem cell factor; BFU-E, burst-forming unit-erythroid; CFU-GM, colony-forming unit-granulocyte macrophage; CFU-GEMM, colony-forming unit-granulocyte erythrocyte monocyte macrophage.

PEBP2β causes familial platelet disorder with predisposition to AML (FPD/AML), which is characterized by decreased platelet count and propensity to develop AML (19).

MDS are clonal hematological disorders derived from gene alteration at a level of HSC (20), which are characterized by ineffective hematopoiesis, dysplastic morphology of blood cells, and high possibility to transit to AML. A number of genetic or epigenetic alterations involved in the pathogenesis of MDS have been identified as follows: activating point mutations of signaling molecules such as N-RAS and Flt3 (21, 22); deletion, point mutation, and/or silencing of cell cycle inhibitory molecules such as p15, p16, and p53 (23–25); deletion, point mutation, and generation of chimeric genes for transcriptional factors such as Evi1, IRF-1, AML1 (26–28), and point mutations of the nucleolar protein (Nucleophosmin) (29). Among them, the point mutations of *AML1* were found in 15–17% of patients with sporadic MDS/AML (high risk MDS and AML following MDS) (3, 30). Previously, point mutations of AML1 were intensively screened in the N-terminal region, including the Runt domain in patients with AML and MDS, and the researchers found several point mutations, most of which disrupts DNA binding activity of AML1 but not the interaction with PEBP2β (3). In addition, recent reports have revealed that about 50% of point mutations are detected in the C-terminal region in MDS/AML. In addition, a C-terminal *AML1* point mutation was also detected FPD/AML (30, 31). Most of the C-terminal mutations of AML1 lead to the premature termination yielding the C-terminally truncated form of AML1, which inhibits transcriptional activity of AML1.

Thrombopoietin (TPO) is a crucial regulator of megakaryopoiesis and platelet production. It stimulates both megakaryocyte progenitor cell growth and subsequent maturation *in vitro* and *in vivo* (32). In accord with these data, knock-out mice for TPO or its receptor c-*mpl* both revealed severely impaired megakaryopoiesis and platelet reduction (about 5% of normal mice) without apparent abnormality in erythropoiesis, granulopoiesis, and lymphopoiesis, suggesting that a physiologic role of the TPO/c-Mpl system is restricted to the megakaryocytic lineage. However, in the later study, the total number of HSCs was found to be reduced in the bone marrow of c-Mpl$^{-/-}$ mice (57). Also, c-Mpl$^{-/-}$ HSCs revealed severely decreased reconstitution activity in transplantation experiments. These results indicate that TPO/c-Mpl-mediated signaling also plays an important role in the growth and survival of HSCs as well as in megakaryopoiesis (33, 34).

Considering the fact that both AML1 and TPO/c-Mpl signaling play crucial roles in the growth and survival of HSCs as well as in megakaryopoiesis, we speculate the transcriptional regulation by AML1 might have some influence on TPO/c-Mpl signaling. So, we here examined the effects of AML1 on the c-Mpl transcription using the promoter analyses. Also, we analyzed the biologic effects of AML1dC on c-Mpl expression in HSC and megakaryocytes and on megakaryocytic differentiation.

EXPERIMENTAL PROCEDURES

Reagents and Antibodies—Recombinant human (h) interleukin-6 (hIL-6), murine (m) IL-3, murine stem cell factor (mSCF), human thrombopoietin (hTPO), human erythropoietin, and an anti-mouse c-Mpl monoclonal antibody were provided by Kirin Brewery Co. (Tokyo, Japan). Human flt3-ligand was purchased from PeproTech (London, UK). Fluorescein isothiocyanate (FITC)-conjugated rat IgG1 and biotinylated rat IgG2b were purchased from Immunotech (Marseilles, France). Biotinylated anti-lineage (Lin) antibodies (Abs) against Gr-1 (RB6–8C5), B220 (RA3–6B2), CD3 (145–2C11), Mac1 (M1/70), and Ter119 (TER119), FITC-labeled anti-Sca-1(D7), phycoerythrin-labeled anti-c-Kit (2B8), phycoerythrin-conjugated anti-Rat Igλ (B46–5), and streptavidin-PerCP-Cy5.5 were purchased from BD Biosciences. The anti-AML-1 Ab (N-20) and normal goat IgG were purchased from Santa Cruz Biotechnology (Santa Cruz, CA).

Plasmid Constructs—The expression vectors for AML1b and AML1-MTG8 (pRCCMV-AML1b and pRCCMV-AML1-MTG8) were kindly provided by Dr. Kitabatashi (National Cancer Center Research Institute, Tokyo, Japan) (35). AML1dC, lacking the C terminus of AML1b (amino acids from 224 to 453), was obtained by the PCR method. Retrovirus expression vectors for AML1b and AML1dC were generated by subcloning these cDNAs into the Mie vector (pMSCV-IRES-EGFP). The expression vector for PEBP2β was provided by Dr. N. A. Speck (Dartmouth Medical School, Hanover, NH) (36).

Luciferase Assays—To construct reporter genes for the c-*mpl* promoter, various PCR products were subcloned into the luciferase plasmid, PSP72-Luc (37). Luciferase assays were performed with a dual luciferase reporter system (Promega, Madison, WI) as described previously (37). In short, 293T cells (2×10^5 cells) cultured in DMEM containing 10% fetal bovine serum (FBS) were seeded into a 60-mm dish and transfected with the effector genes (2 μg) and reporter gene (2 μg) together with pRL-CMV-Rluc (5 ng), an expression vector for *Renilla* luciferase, by the calcium phosphate coprecipitation method. After 12 h, the cells were washed and serum-deprived for 24 h. Then the cells were lysed and subjected to the measurement of the firefly and *Renilla* luciferase activities on a luminometer LB96P (Berthold Japan, Tokyo, Japan). The relative firefly luciferase activities were calculated by normalizing transfection efficiencies according to the *Renilla* luciferase activities. To perform luciferase assays in HeLa cells, we used a FuGENE 6 (Roche Applied Science) for transfection. The experiments were performed in triplicate, and the similar results were obtained from at least three independent experiments.

Electrophoretic Mobility Shift Assay (EMSA)—EMSA was performed as described previously (38). One probe used as a positive control contained the reported AML1-binding sequence (39). One more probe contained the proximal putative AML1-binding sequence in the human c-*mpl* promoter (−135/−116, numbered from the first ATG). For competition assays, unlabeled oligonucleotides containing wild-type (WT) (TGTGGT) or mutated (MT) (TGTTAG) AML1-binding site were added to the DNA-binding reaction mixtures. The sequences of the oligonucleotides are as follows: WT AML1, 5′-CGAGTATTGTGGTTAATACG-3′; MT AML1, 5′-CGAGTATTGTTAGTAATACG-3′; c-*mpl* (−135/−116) WT, 5′-ACCCCAGTGTGGTCTGGATG-3′; and c-*mpl* (−135/−116) MT, 5′-ACCCCAGTGTTAGCTGGATG-3′.

Chromatin Immunoprecipitation (ChIP) and ReChIP Assays—ChIP assays were performed with a ChIP assay kit (Upstate Biotechnology Inc.). Briefly, 1×10^7 cells were fixed with 1% formaldehyde for 10 min. Cross-links were quenched with 125 mM glycine. After isolation of the nuclear extract, chromatin was sonicated to shear DNA to the length between 200 and 1000 bp. After sonication, AML1-DNA-binding complexes were immunoprecipitated with the anti-AML1 Ab or control goat IgG. The immunoprecipitated DNA was eluted and subjected to the PCRs using AmpliTaq Gold (PerkinElmer Life Sciences), in the following thermal cycling conditions: 94 °C for 10 min, 30 cycles of 94 °C for 30 s, 65 °C for 30 s, and 72 °C for 30 s, followed by 72 °C for 10 min. The sequences of the primer set for the human c-*mpl* promoter are as follows: sense, 5′-TTTCCCCAGTGTGGTCTGGATGG-3′; antisense, 5′-TTTGCCTTAGCCCATCCTCCCTT-3′. PCR products were electrophoresed on agarose gels and visualized by staining with SYBR Green I (BioWhittaker Molecular Applications, Rockland, ME). In the sequential ChIP (ReChIP) experiments, we performed a first ChIP with the anti-AML1 Ab. Immunoprecipitated complexes were eluted by incubation for 30 min at 37 °C in 50 μl of 10 mmol/liter dithiothreitol. After centrifugation, the supernatant was diluted 20 times with ReChIP buffer (1% Triton X-100, 2 mmol/liter EDTA, 150 mmol/liter NaCl, 20 mmol/liter Tris-HCl, (pH 8.0)) and subjected to the second re-immunoprecipitation and the ChIP procedure. In the ReChIP analysis, PCRs were performed with 35 cycles of amplification (40, 41).

Purification of Murine c-Kit$^+$Sca1$^+$Lin$^-$ (KSL) Cells—Bone marrow cells were harvested from 8- to 10-week-old C57BL/6 mice, and mononuclear cells were isolated by density gradient centrifugation. After staining with biotinylated anti-Lin Abs, an FITC-conjugated anti-Sca1 Ab, a phycoerythrin-conjugated anti-c-Kit A, and a streptavidin-PerCP-Cy5.5, KSL cells were sorted on FACS Aria (BD Biosciences).

Preparation of the Conditioned Medium Containing Retrovirus Particles—Conditioned medium containing high tighter retrovirus particles was prepared as reported previously (38). Briefly, retrovirus plasmid DNA was transfected into retrovirus packaging cell line 293gp along with a vesicular stomatitis virus-G envelope expression plasmid by the calcium phosphate coprecipitation method. After 48 h, cultured supernatant was collected and concentrated by 100-fold in volume.

Retrovirus Transfection into Murine Hematopoietic Stem/Progenitor Cells—Purified KSL cells were cultured in DMEM containing 10% FBS, mSCF (100 ng/ml), and hTPO (100 ng/ml). Then the cells were seeded into the culture plates coated with Retronectin (TAKARA BIO, Shiga, Japan) and cultured with conditioned medium containing retrovirus and Polybrene (10 μg/ml) in the presence of mSCF (100 ng/ml) and hTPO (100 ng/ml). After 24 h, cells were washed and cultured in DMEM containing 10% FBS, mSCF (50 ng/ml), human flt3-ligand (30 ng/ml), and hIL-6 (50 ng/ml).

Flow Cytometry—Two days after retrovirus infection, GFP$^+$ cells were sorted by FACS Aria (BD Biosciences). Cell surface marker analyses were performed with FACSCalibur (BD Biosciences). DNA content of cultured cells was examined by staining with propidium iodide and analyzed by the same device. FACS data were analyzed by FlowJo software (TreeStar, Ashland, OR). To analyze TPO-dependent tyrosine phosphorylation of STAT5, we used BD Phosflow™ Technology (BD Biosciences). Two days after retrovirus infection, Mock-, AML1dC-, and AML1b-transduced cells were cultured in DMEM containing 2% FBS without cytokines for 4 h. The cytokine-deprived cells were then stimulated with hTPO (100 ng/ml) for 15 min. Fixed samples were stained with Alexa Fluor®647 STAT5 (pY694) and analyzed by FACS Aria (BD Biosciences).

RT-PCR—For RT-PCR, total RNA was isolated from 7×10^3 GFP$^+$ cells and was reverse-transcribed into cDNA with oligo(dT) primers (Pharmacia, Piscataway, NJ) using SuperScript II reverse transcriptase (Invitrogen). PCR was performed in a total volume of 50 μl using 4 μl of the cDNA product as a template and 1 μl of Advantage cDNA polymerase mix (Clontech). The primer sets to amplify murine c-*mpl* and β-actin are as follows: c-*mpl*, 5′-CCTACTGCTGCTAAAGTGGCAAT-3′ and 5′-CAATAGCTTAGTGGTAGGTAGGA-3′; β-actin, 5′-CATCACTATTGGCAACGAGC-3′ and 5′-ACGCAGCTCAGTAACAGTCC-3′. Cycling conditions were 94 °C for 1 min, followed by 22–35 cycles of 94 °C for 30 s and 68 °C for 3 min, followed by 68 °C 5 min. The PCR products were electrophoresed on agarose gels, and their amounts were evaluated by staining with SYBR Green I (BioWhittaker Molecular Applications, Rockland, ME).

OP9 System to Develop Hematopoietic Cells from Murine ES Cells—E14tg2a ES cells and OP9 stromal cells were maintained as described previously (42, 43). To induce differentiation toward hematopoietic cells, ES cells were deprived of leukemia inhibitory factor and seeded onto confluent OP9 cells in 6-well plates at a density 10^4 cells/well in α-minimum essential medium supplemented with 20% FBS. After 4.5 days, Flk-1$^+$ cells were sorted by FACS or the cells were harvested by 0.25% trypsin/EDTA, and whole cell suspensions were transferred into a new 10-cm dish and incubated in 37 °C for 30 min to remove adherent OP9 cells. The collected floating cells were replated onto OP9 cells at a density 1×10^4 cells/well of 6-well plate or 6×10^4 cells/10-cm dish and cultured under the indicated conditions.

Tetracycline (Tet)-regulated Inducible Expression of AML1dC in ES Cells—To inducibly express AML1dC in ES cells, we utilized a Tet-Off system as reported previously (44, 45), in which transcription of the target mRNA is initiated by the removal of Tet from the culture medium. Briefly, we initially introduced pCAG20-1-tTA and pUHD10-3-puro by electroporation (800 V, 3 microfarads) and selected one clone designated E14 by the culture with 1 μg/ml of Puro and/or 1 μg/ml of Tet, in which the Tet-regulatory system works most effectively. We further transfected pUHD10–3-AML1dC-GFP, which can inducibly express AML1dC and GFP as a single mRNA through the internal ribosome entry site in response to the Tet removal, together with the neomycin-resistant plasmid pcDNA3.1-neo. After the culture with G418 (0.4 mg/ml) in the Tet$^+$ medium, we selected several clones that can inducibly express GFP in response to the Tet deprivation. Subsequently, we examined the Tet-regulated expression of AML1dC in the

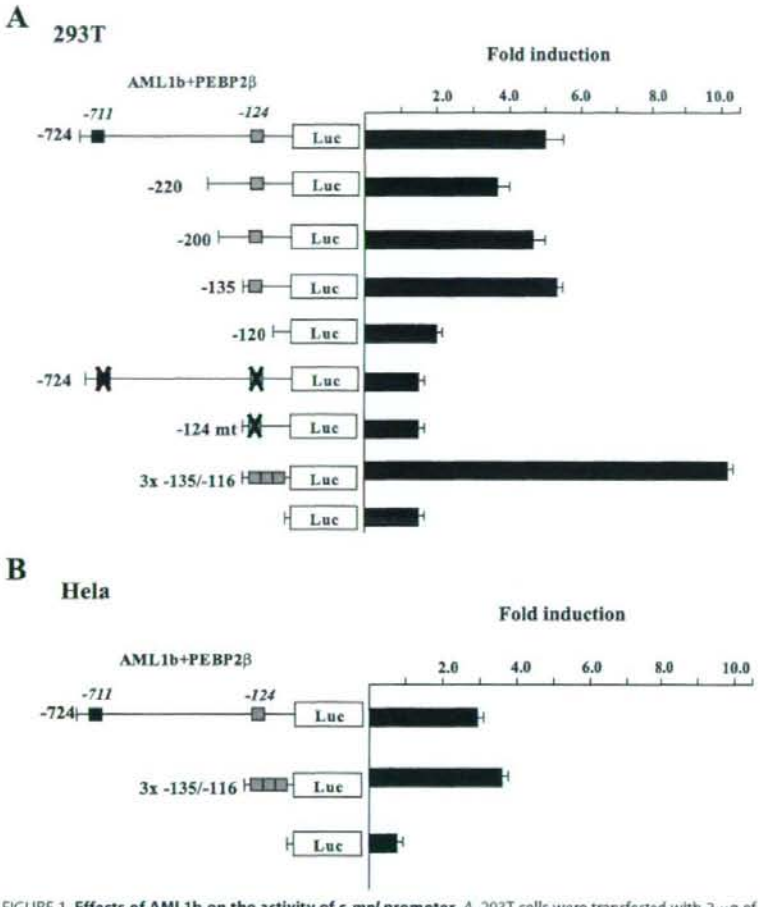

FIGURE 1. **Effects of AML1b on the activity of c-*mpl* promoter.** *A*, 293T cells were transfected with 2 μg of AML1b, PEBP2β, and 2 μg of indicated reporter gene. The relative firefly luciferase (*LUC*) activities were calculated by normalizing transfection efficiencies according to the *Renilla* luciferase activities. The results are shown as the means ± S.D. of triplicate cultures. *B*, HeLa cells were transfected with 0.5 μg of AML1b and PEBP2β and 1 μg of reporter genes by FuGENE 6.

proximal 724 bp of the c-*mpl* promoter using 293T cells. As shown in Fig. 1*A*, WT AML1b activated the −724 construct about 5.0-fold in the presence of its heterodimerization partner, PEBP2β. As there were two putative AML1-binding sites (TGTGGT) in the −724 construct, we further constructed several deletion mutants. Although deletion of the distal AML1-binding site (−711) and extended deletion up to −135 bp did not influence the c-*mpl* promoter activation by AML1b, the −120 construct further lacking the proximal AML1-binding site (−124) was scarcely activated by AML1. In addition, AML1b could not activate −124mt construct, in which the proximal AML1-binding site was changed from TGTGGT to TGTTAG. Furthermore, AML1 activated the 3× −135/−116 construct containing three tandem repeats of the proximal AML1-binding site and minimal JunB promoter over 10-fold. Similar results were obtained from luciferase assays using HeLa cells (Fig. 1*B*). These results suggest that AML1 may regulate the expression of c-*mpl* through the proximal AML1-binding site in the promoter.

AML1 Transcriptionally Regulates the c-mpl Promoter—To analyze whether AML1 directly binds to the proximal AML1-binding sequence in the c-*mpl* promoter, we performed EMSA with the corresponding c-*mpl* (−135/−116) probe. Also, one more probe with the reported AML1-binding sequence (39, 46) was used as a positive control. Nuclear extracts were isolated from 293T cells that were transfected with PEBP2β with or without AML1b. As compared with the nuclear extract from AML1b-untransfected 293T cells (Fig. 2*A*, *lane 1*), that from AML1b-transfected cells formed two additional complexes with the c-*mpl* (−135/−116) probe (*lane 2*), and their mobilities were almost the same with that detected by the positive control probe (*lane 7*). These complexes were abolished by the WT competitor (Fig. 2*A*, *lanes 3* and *8*) but not by the MT competitor (*lanes 4* and *9*). Furthermore, these complexes were supershifted by the anti-AML1 Ab (Fig. 2*A*, *lanes 5* and *10*). These data indicate that these complexes were formed in a sequence-specific manner and contained AML1. To further test whether endogenous AML1 binds to the *c-mpl* promoter *in vivo*, we conducted ChIP assays using the anti-AML1 Ab. To obtain enough numbers of hema-

Tet$^+$ and Tet$^-$ medium in these clones, and several clones were subjected to further analyses.

Colony Assays—Two days after retrovirus infection, GFP$^+$ cells (1000 cells/35-mm dish) were cultured in the methylcellulose media M3234 (Stem Cell Technologies, Vancouver, British Columbia, Canada) containing the indicated cytokines. The number of CFU-GM was counted on day 7 and those of BFU-E and CFU-GEMM on day 12.

RESULTS

Function of AML1b on c-mpl Promoter Activity—To examine the effect of AML1 on TPO/c-Mpl-mediated signaling, we initially examined whether AML1 transcriptionally regulates the expression of c-*mpl*. For this purpose, we performed luciferase assays with the −724 construct, a reporter gene containing the

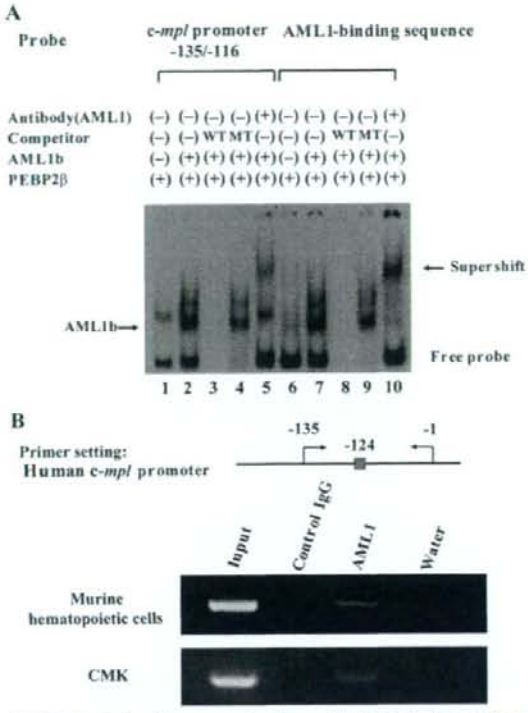

FIGURE 2. **Analysis of the responsive element to AML1b in the c-*mpl* promoter.** *A*, EMSA was performed with the probe containing putative AML1-binding sequence in the human c-*mpl* promoter or known AML1-binding sequence (positive control). Nuclear extract was isolated from 293T cells transfected with the indicated genes and subjected to EMSA. In competition assays, a 1000-fold molar excess of unlabeled wild-type or mutant competitor oligonucleotide was added to the binding mixture. *B*, location of AML1-binding site and the primer set in the c-*mpl* promoter utilized for the ChIP assay are indicated. The nuclear extract was isolated from primary cultured murine hematopoietic cells and CMK cells, and the chromatin was sonicated. Then AML1-DNA-binding complexes were immunoprecipitated with the anti-AML1 Ab (N-20) or control goat IgG. The immunoprecipitated DNA was eluted and subjected to the PCR analyses. PCR products were electrophoresed on agarose gels and visualized with SYBR Green staining.

topoietic cells, we separated Lin^- cells and cultured with mIL-3 and hTPO for 3 days. Nuclear extracts were isolated from 1×10^7 cultured cells. As shown in Fig. 2*B*, the c-*mpl* promoter, including the proximal AML1-binding site, was immunoprecipitated by the anti-AML1 Ab but not by control IgG (Fig. 2*B*). Similar results were also observed using the nuclear extract obtained from a human megakaryocytic cell line CMK (Fig. 2*B*). Together, these data indicate that endogenous AML1 bind to the proximal AML1-binding site in the c-*mpl* promoter and suggest that AML1 might regulate its transcription.

AML1dC Dominant-negatively Suppresses AML1 Function—Next, we examined the effects of a mutant of AML1b, AML1dC, on the c-*mpl* promoter activity. AML1dC is a C-terminal deletion mutant of AML1b (Fig. 3*A*), which was originally identified in a patient with MDS (30). Harada *et al.* (30) reported that this mutant suppressed transactivation activity of AML1 for macrophage colony-stimulating factor receptor. As was the case with the macrophage colony-stimulating factor receptor, AML1dC dose-dependently suppressed AML1b/PEBP2β-induced c-*mpl* promoter activity in 293T cells as efficiently as AML1-MTG8, which is known to act as a dominant-negative repressor of AML1 (Fig. 3*B*). To clarify how AML1dC inhibits AML1 activity, we performed EMSA with the c-*mpl* (−135/−116) probe. As shown in Fig. 3*C*, only 2.5 μg of cotransfected AML1dC was able to effectively cancel the DNA-binding complex formed by 10 μg of transfected wild-type AML1b, which was more prominent when 10 μg of AML1dC was cotransfected (Fig. 3*C*, *lanes 3* and *4*). These results suggest that AML1dC dominant-negatively suppresses the function of AML1 by inhibiting its DNA binding activity.

AML1dC Enhances c-Mpl Expression in Hematopoietic Stem/Progenitor Cells—Because TPO/c-Mpl signaling plays an important role in the proliferation and survival of hematopoietic stem/progenitor cells (33, 34), we next examined the function of AML1 in the c-Mpl regulation in hematopoietic stem/progenitor cells. For this purpose, we transduced AML1dC and AML1b into murine KSL cells with a retrovirus system (Fig. 4*A*). Two days after retrovirus infection, we sorted retrovirus-transduced cells, which are detected by the GFP expression, and performed RT-PCR analysis. Unexpectedly, in contrast to the result of luciferase assays in 293T and HeLa cells that suggests AML1 positively regulates the c-*mpl* expression, AML1dC-transduced cells expressed c-*mpl* mRNA more abundantly than mock-transduced cells in several repeated experiments (representative result is shown in Fig. 4*B*). In accord with this result, FACS analysis showed that the c-Mpl was more intensely expressed in AML1dC-transduced cells than in mock-transduced cells (mean fluorescent intensity, AMLdC 79.8 *versus* Mock 61.5) (Fig. 4*C*). On the other hand, c-*mpl* mRNA and cell-surface c-Mpl expression were suppressed in AML1b-transduced cells than those in Mock-transduced cells (mean fluorescent intensity: AMLb 49.0 *versus* Mock 61.5) (Fig. 4, *B* and *C*).

AML1dC Enhances c-Mpl Expression in Hematopoietic Cells That Derived from Murine ES Cells—To further explore the effects of AML1dC on the c-Mpl expression during the development of hematopoietic stem/progenitor cells, we utilized the Tet-Off system in the OP9 system. In the OP9 system, after deprivation of leukemia inhibitory factor from the culture medium, Flk-1^+ hemangioblasts that have both the potential to develop into hematopoietic cells and endothelial cells develop from ES cells after 4.5 days, and definitive hematopoietic stem/progenitor cells appear after 8.5 days (Fig. 5*A*) (42, 43). After sorting Flk-1^+ cells on day 4.5, we inducibly expressed AML1dC by depriving Tet from the culture medium, cultured for 4 days, and performed FACS analysis on day 8.5. After the culture with Tet, 50.5% of AML1dC-transduced ES cells were positive for c-Mpl in the GFP-negative fraction (Fig. 5*B*, *upper left panel*). In contrast, after the culture without Tet, 77.0% of AML1dC-transduced ES cells were positive for c-Mpl in the GFP-positive fraction (Fig. 5*B*, *upper right panel*). Similar results were obtained in other clones of AML1dC (data not shown). Tet deprivation by itself did not influence c-Mpl expression in mock-transduced ES cells (data not shown). Together with the results obtained from AML1dC- and

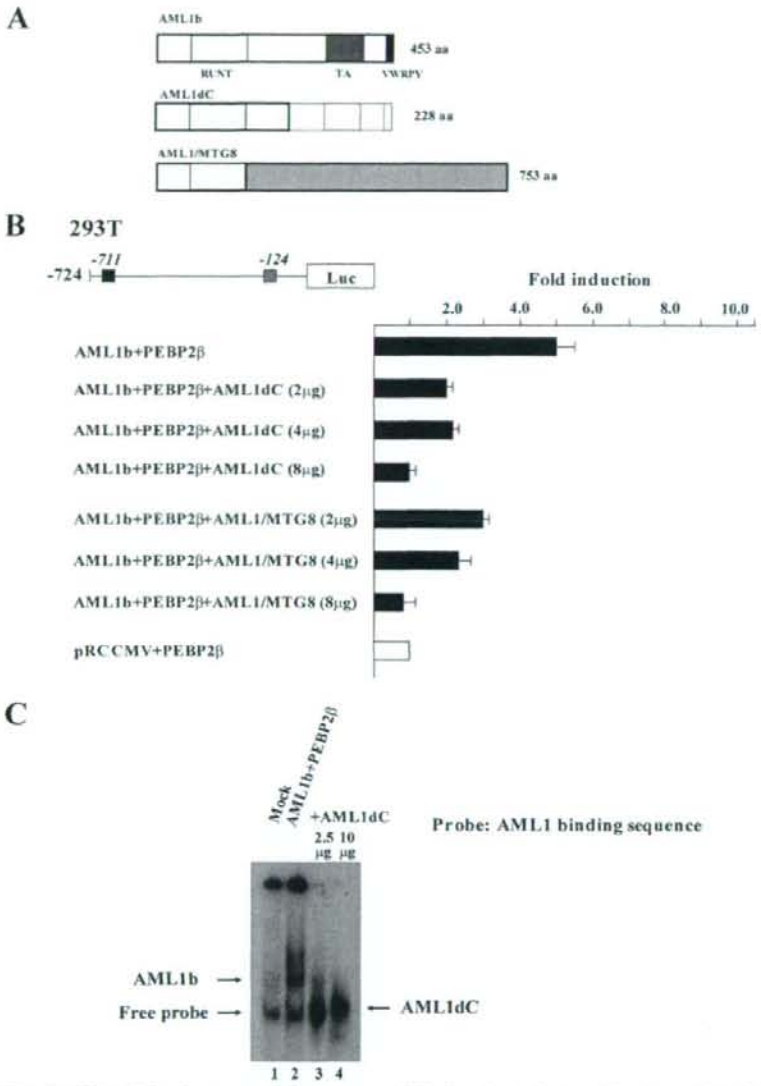

FIGURE 3. **AML1dC dominant-negatively suppresses AML1 function.** *A, horizontal bars* show WT AML1b (453 amino acids (*aa*)), C-terminal deletion mutant of AML1b (288 amino acids), and AML1/MTG8 (753 amino acids). In the case of AML1dC, the insertion of ACCGT into 669–670 causes frameshift mutation and results in truncation of WT AML1b. *RUNT* indicates the runt domain; *TA* indicates the transactivation domain; *VWRPY* indicates the VWRPY motif. *B*, 293T cells were transfected with 2 μg of AML1b, PEBP2β, and indicated doses of AML1dC or AML1/MTG8. The results are shown as the means ± S.D. of triplicate cultures. *C*, EMSA was performed with the probe containing AML1-binding sequence. Nuclear extracts were isolated from 293T cells transfected with empty vector (10 μg) or AML1b (10 μg), PEBP2β (10 μg), and indicated doses of AML1dC.

AML1b-transduced KSL cells, these results indicate that wild-type AML1 is a negative regulator of the *c-mpl* transcription in hematopoietic stem/progenitor cells.

Haploinsufficiency of AML1 Also Enhances c-Mpl Expression in ES-derived Hematopoietic Cells—AML1dC might influence the expression of c-Mpl on hematopoietic stem/progenitor cells not only as a dominant-negative mutant but also through the unknown mechanisms. So, it is important to examine the expression of c-Mpl on hematopoietic stem/progenitor cells, in which the expression of AML1 was simply reduced. For this purpose, we developed hematopoietic stem/progenitor cells from murine AML1$^{+/-}$ ES cells and examined the c-Mpl expression on these cells, because AML1-null-ES cells cannot differentiate into definitive hematopoietic cells (47). As a result, we found that early hematopoietic cells that derived from AML1$^{+/-}$ ES cells expressed c-Mpl more intensively than those that developed from WT ES cells (mean fluorescent intensity, AML1$^{+/-}$ 129.8 *versus* WT 27.0) (Fig. 5*C*). This result again suggests that AML1 is a negative regulator of c-Mpl expression in hematopoietic stem/progenitor cells.

AML1dC Does Not Influence the c-Mpl Expression in Megakaryocytes or Their Maturation—Except for immature hematopoietic cells, c-Mpl is exclusively expressed on megakaryocytic cells and plays essential roles in megakaryopoiesis and subsequent platelet production. So we next analyzed the effects of AML1dC on megakaryocytic maturation and the c-Mpl expression on mature megakaryocytes. For this purpose, we cultured AML1dC-transduced ES clones in the presence of TPO for 12.5 days (Fig. 5*D*). On day 12.5, morphologic analysis showed that AML1dC-transduced ES cells were able to possess polyploid nucleus, which is characteristic of mature megakaryocytes, regardless of the presence or absence of Tet (Fig. 5*D*). Also, FACS analysis on day 12.5 showed that Tet deprivation neither inhibited polyploidization of megakaryocytes (Fig. 5*E*) nor their c-Mpl expression (Fig. 5*B*, *lower panels*) in AML1dC-transduced ES cells.

AML1 Forms Different Transcriptional Complex on the c-mpl Promoter in Hematopoietic Stem/Progenitor Cells and Megakaryocytes—Our findings suggested AML1 differentially regulates the c-Mpl expression in hematopoietic stem/progenitor cells and megakaryocytic cells. Because AML1 forms a

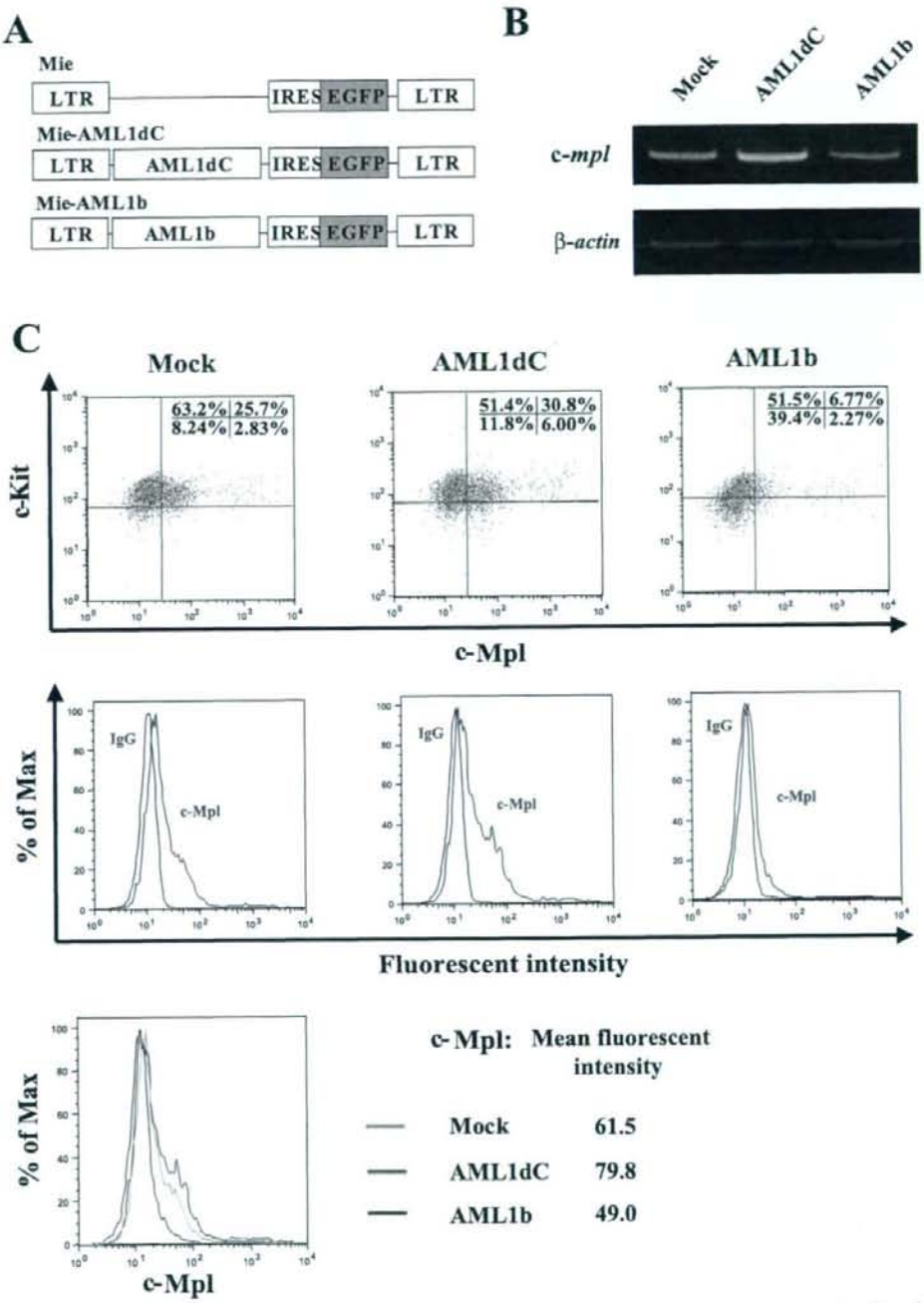

FIGURE 4. **Analysis of the c-Mpl expression in murine hematopoietic stem/progenitor cells.** *A*, structure of Mie (Mock), Mie-AML1dC, and Mie-AML1b retroviruses. *B*, 2 days after retroviral transfection, GFP$^+$ cells were sorted and subjected to RT-PCR to examine the expression of c-*mpl* and β-actin mRNA. *C*, at the same point, the surface phenotype of GFP$^+$ fraction of Mie, Mie-AML1dC, and Mie-AML1b-transduced cells was examined by FACS. Dot plots of cell-surface expressions of c-Kit and c-Mpl (*upper panels*) are shown. Histogram plots and mean fluorescent intensities of c-Mpl expression (*middle* and *lower panels*) are shown. *LTR*, long terminal repeat; *IRES*, internal ribosome entry site.